




# Asynchronous Localization for UASNs: An Unscented Transform-Based Method

Jing Yan , *Member, IEEE*, Haiyan Zhao, Yiyin Wang, Xiaoyuan Luo , and Xinping Guan , *Fellow, IEEE*

**Abstract**—This letter is concerned with an asynchronous localization issue for underwater acoustic sensor networks (UASNs), subject to asynchronous clocks and stratification effects in physical channels. A novel unscented transform-based localization algorithm is proposed to estimate the positions of sensor nodes. Instead of linearizing the measurement equations, the proposed algorithm employs the unscented transform to compute the Jacobian matrix to reduce the linearization errors. Particularly, the ray-tracing approach is adopted to model the stratification effect. Moreover, the convergence analysis and Cramér–Rao lower bound for the algorithm are also provided. Simulation results show that the proposed algorithm can effectively improve the estimation accuracy as compared with the existing works.

**Index Terms**—Underwater acoustic sensor networks (UASNs), localization, synchronization, unscented transform.

## I. INTRODUCTION

**M**OST applications of acoustic sensor networks (UASNs) demand accurate locations of sensor nodes [1]. However, the weak characteristics of acoustic communications make underwater localization more challenging as compared with terrestrial sensor networks. For instance, the clocks in UASNs are asynchronous, due to the unavailability of global positioning system (GPS) and the high propagation delays of acoustic communications. Moreover, the water medium is inhomogeneous, leading to the stratification effect of the sound speed. Thereby, the localization algorithms [2]–[5] developed for terrestrial networks cannot be directly applied to UASNs.

On the aspect of asynchronous localization in inhomogeneous water medium, some joint localization and synchronization algorithms have been proposed. For instance, a joint solution to

localization and synchronization was presented in [6]. In [7], the sound velocity profile was employed to compensate the stratification effect. It is noted that, the localization and synchronization in [6], [7] are performed at different phases, which can increase the ranging errors and ultimately reduce the estimation accuracy. Inspired by this, a unified framework was given in [8] where the localization and synchronization tasks can be achieved simultaneously. Without consideration of the stratification effect, [9] attempted to use an autonomous vehicle to aid the localization process. Our previous work [10] provided a mobility prediction based asynchronous localization algorithm. In these studies, the first-order linearization is required to compute the Jacobian matrix, through which linear measurements can be obtained. However, the calculation of the Jacobian matrix is not an easy task. Meanwhile, the first-order linearization can introduce large model errors [11]. In order to reduce model errors, it is necessary to relax the linearization requirement. We notice that an approximate method called the *unscented transform* [12] can give a promising solution. The merits of the unscented transform are that the Jacobian matrix calculation is unnecessary and the second-order Taylor expansion accuracy can be guaranteed. Per our understanding, how to present an unscented transform based solution that involves asynchronous clock and stratification effect to improve the estimation accuracy of UASNs is largely unexplored.

This letter proposes an unscented transform method for the localization of UASNs. With consideration of the asynchronous clock and the stratification effect, we first establish the relationship between the propagation delay and the position. Then, an asynchronous localization algorithm is proposed. Main contributions lie in two aspects: 1) we employ the unscented transform to compute the Jacobian matrix. Instead of linearization techniques required by [6]–[9], the unscented transform in this letter can reduce the linearization errors. 2) We adopt the ray tracing approach to model stratification effect. Compared with [10], [11], the proposed method in this letter can compensate the influence of the stratification effect.

## II. SYSTEM MODEL

A network architecture that comprises of three types of nodes is considered. Particularly, *surface buoys* act as “satellite” nodes, whose role is to provide localization service for anchor nodes. *Anchor nodes* make direct contact with buoys, whose clocks are synchronized and the locations are pre-known. *Ordinary nodes* are low complexity sensor nodes which cannot make direct contact with buoys. Of note, the position of the ordinary nodes

Manuscript received December 23, 2018; accepted February 24, 2019. Date of publication February 28, 2019; date of current version March 13, 2019. This work was supported in part by the NSFC under Grants 61873345 and 61603328, in part by the Youth Talent Support Program of Hebei under Grant BJ2018050, in part by Returned Overseas Chinese Scholar Foundation of Hebei under Grant C201829, and in part by the Open Project of Xiamen University under Project UAC201803. The associate editor coordinating the review of this manuscript and approving it for publication was Dr. Ioannis D. Schizas. (*Corresponding author: Jing Yan.*)

J. Yan is with the Institute of Electrical Engineering, Yanshan University, Qinhuangdao 066004, China, and also with the Key Laboratory of Underwater Acoustic Communication and Marine Information Technology, Ministry of Education, Xiamen 361005, China (e-mail: jyan@ysu.edu.cn).

H. Zhao and X. Luo are with the Institute of Electrical Engineering, Yanshan University, Qinhuangdao 066004, China (e-mail: hyzhao@stumail.ysu.edu.cn; xylo@ysu.edu.cn).

Y. Wang and X. Guan are with the Department of Automation, Shanghai Jiao Tong University, Shanghai 200240, China (e-mail: yiyinwang@sjtu.edu.cn; xpguan@sjtu.edu.cn).

Digital Object Identifier 10.1109/LSP.2019.2902273

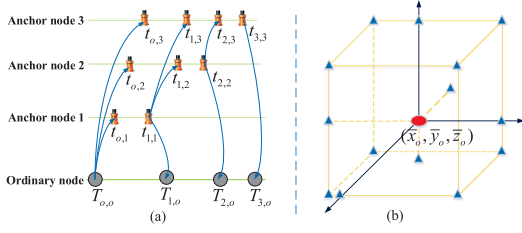


Fig. 1. (a) Two-way transmission process. (b) Selection of a set of sigma points with an arbitrary prior means  $\bar{x}_0, \bar{y}_0$  and  $\bar{z}_0$ .

are required to be calculated. Without loss of generality, only one ordinary node is considered here.

Different from the simplified model in [10], [11], [13], a clock model including both the skew and offset is considered

$$T = \alpha t + \beta, \quad (1)$$

where  $T$  is the measured time on the ordinary node,  $t$  is the real time,  $\alpha$  is the clock skew, and  $\beta$  is the clock offset.

Similar to [14], it is assumed that the stratification effect is depth dependent. Thus, the sound velocity is formulated as  $C(z) = b + \bar{a}z$ , where  $b$  is the sound speed at the water surface,  $\bar{a}$  is the update scalar depending on the environment, and  $z$  denotes the depth. Accordingly, the propagation delay between the receiver point A and the sender point B is

$$\tau_{A,B} = -\frac{1}{\bar{a}} \left( \ln \frac{1 + \sin \theta_B}{\cos \theta_B} - \ln \frac{1 + \sin \theta_A}{\cos \theta_A} \right), \quad (2)$$

where  $\theta_A = \beta_0 + \alpha_0$  and  $\theta_B = \beta_0 - \alpha_0$  are the ray angles at the point A and the point B, respectively, as described in [14]. Particularly,  $\beta_0 = \arctan \frac{z_B - z_A}{\sqrt{(x_B - x_A)^2 + (y_B - y_A)^2}}$  denotes the angle of the straight line between the point A and the point B, with respect to the horizontal axis.  $\alpha_0 = \arctan \frac{0.5\bar{a}\sqrt{(x_B - x_A)^2 + (y_B - y_A)^2}}{b + 0.5\bar{a}(z_B + z_A)}$  denotes the angle, at which the ray trajectory deviates from this straight line. Of note,  $(x_B, y_B, z_B)$  and  $(x_A, y_A, z_A)$  represents the position of the point A and the point B, respectively.

### III. DESIGN OF ASYNCHRONOUS LOCALIZATION

The position of the ordinary node is denoted by  $(x_o, y_o, z_o)$ , and the position of the anchor node  $n$  is  $(x_n, y_n, z_n)$  for  $\forall n \in \{1, 2, 3\}$ . Particularly, the ordinary node knows the IDs of all anchor nodes by assuming an initialization procedure [11]. It is noted that, the depth (i.e.,  $z_o$ ) can be acquired through depth units. Thereby, the asynchronization localization problem is transformed into the estimation of  $x_o$  and  $y_o$ .

#### A. Unscented Transform Based Algorithm

After a complete transmission round (see Fig. 1(a)), the collected time stamps are denoted by  $\{t_{o,n}, t_{n,o}, T_{n,o}\}_{n=1}^3$  and  $\{t_{j,\bar{n}}\}_{\bar{n}=2, j=1}^{\bar{n}-1}$ . Note that the ordinary node sends out an initiator message at the time stamp  $T_{o,o}$ , and  $t_{o,n}$  is the time stamp when the anchor node  $n$  receives the message from the ordinary node. Particularly,  $t_{n,o}$  is the time stamp when the anchor node  $n$  sends out its message.  $T_{n,o}$  is the time stamp when the ordinary node receives reply from the anchor node  $n$ , and  $t_{j,\bar{n}}$  is the time stamp when the anchor node  $\bar{n}$  receives the message from the anchor node  $j$ . For  $n \in \{2, 3\}$  and  $j \in \{1, \dots, \bar{n} - 1\}$ , we

define the following time differences

$$\Delta \mathcal{T}_{\bar{n},j} = t_{o,\bar{n}} - t_{o,j}, \Delta \mathcal{T}_{j,\bar{n}} = (t_{j,\bar{n}} - t_{o,\bar{n}}) - (t_{j,j} - t_{o,j}). \quad (3)$$

Suppose that all the nodes have the same measurement quality, and that each local measurement is zero-mean Gaussian with a variance  $\sigma_{mea}^2$ . Then, the relationship between time differences and propagation delays can be established, i.e.,

$$\begin{aligned} \Delta \mathcal{T}_{\bar{n},j} &= \tau_{o,\bar{n}} - \tau_{o,j} + \varpi_{\bar{n},j}, \\ \Delta \mathcal{T}_{j,\bar{n}} &= \tau_{o,j} + \tau_{j,\bar{n}} - \tau_{o,\bar{n}} + \varpi_{j,\bar{n}}, \end{aligned} \quad (4)$$

where  $\tau_{o,\bar{n}}, \tau_{o,j}$  and  $\tau_{j,\bar{n}}$  are the one-way propagation delays, as computed by (2).  $\varpi_{\bar{n},j}$  and  $\varpi_{j,\bar{n}}$  are the measurement noises, satisfying  $\varpi_{\bar{n},j} \sim \mathcal{N}(0, 2\sigma_{mea}^2)$  and  $\varpi_{j,\bar{n}} \sim \mathcal{N}(0, 3\sigma_{mea}^2)$ .

We employ the ray tracing approach to model the stratification effect, then (3) and (4) can be stacked into

$$\underbrace{\begin{bmatrix} \frac{\Delta \mathcal{T}_{2,1}}{2} \\ \frac{\Delta \mathcal{T}_{3,1}}{2} \\ \frac{\Delta \mathcal{T}_{3,2}}{2} \\ \frac{\Delta \mathcal{T}_{1,2}}{\sqrt{6}} \\ \frac{\Delta \mathcal{T}_{1,3}}{\sqrt{6}} \\ \frac{\Delta \mathcal{T}_{2,3}}{\sqrt{6}} \end{bmatrix}}_{:=\varphi} = \underbrace{\begin{bmatrix} \frac{\tau_{o,2} - \tau_{o,1}}{2} \\ \frac{\tau_{o,3} - \tau_{o,1}}{2} \\ \frac{\tau_{o,3} - \tau_{o,2}}{2} \\ \frac{\tau_{o,1} + \tau_{1,2} - \tau_{o,2}}{\sqrt{6}} \\ \frac{\tau_{o,1} + \tau_{1,3} - \tau_{o,3}}{\sqrt{6}} \\ \frac{\tau_{o,2} + \tau_{2,3} - \tau_{o,3}}{\sqrt{6}} \end{bmatrix}}_{:=h(\mathbf{X}, \xi)} + \underbrace{\begin{bmatrix} \frac{\varpi_{2,1}}{2} \\ \frac{\varpi_{3,1}}{2} \\ \frac{\varpi_{3,2}}{2} \\ \frac{\varpi_{1,2}}{\sqrt{6}} \\ \frac{\varpi_{1,3}}{\sqrt{6}} \\ \frac{\varpi_{2,3}}{\sqrt{6}} \end{bmatrix}}_{:=\mathbf{W}} \quad (5)$$

where  $\mathbf{X} = (x_o, y_o, z_o)$ ,  $\xi = [x_1, y_1, z_1; x_2, y_2, z_2; x_3, y_3, z_3]$  and  $\varphi$  is the measurement vector.  $\mathbf{W}$  is the measurement noise, whose mean value and variance are  $\mathbf{r}$  and  $\mathbf{R}$ , respectively.

We use the unscented transform to compute the Jacobian matrix. In the unscented transform, a set of sigma points is chosen with prior means and covariances, as described in Fig. 1(b). It is noted that, the prior means and covariance can be selected arbitrarily, i.e., the true prior information of  $\mathbf{X}$  is not required to be known previously. Substituting these sigma points into (5), the mean and covariance of  $\varphi$  are estimated. Accordingly, the nonlinear measurement (5) can be indirectly transformed into the linear measurement  $\varphi = \mathbf{H}\mathbf{X} + \mathbf{W}$ , where  $\mathbf{H}$  denotes the Jacobian matrix. In the following, we give the detailed localization algorithm.

*Step 1. Selection of the sigma points:* The prior mean of  $\mathbf{X}$  is denoted by  $\bar{\mathbf{X}}$ , whose error covariance matrix is  $\mathbf{P}_{\mathbf{X}\mathbf{X}}$ . Then,  $2m + 1$  sigma points  $\chi_i$  are selected [12], i.e.,

$$\begin{aligned} \chi_i &= \bar{\mathbf{X}}, \quad i = 0 \\ \chi_i &= \bar{\mathbf{X}} + (\sqrt{(m+\lambda)\mathbf{P}_{\mathbf{X}\mathbf{X}}})_i, \quad i = 1 \sim m \\ \chi_i &= \bar{\mathbf{X}} - (\sqrt{(m+\lambda)\mathbf{P}_{\mathbf{X}\mathbf{X}}})_{i-m}, \quad i = m + 1 \sim 2m, \end{aligned} \quad (6)$$

where  $m = 3$  is the state dimension,  $\lambda$  is the scaling parameter, and  $(\cdot)_i$  denotes the  $i$ th column of a matrix.

*Step 2. Iteration update:* Using a weighted sample method, the prior mean  $\bar{\mathbf{X}}$  and the covariance matrix are updated as

$$\bar{\mathbf{X}} = \sum_{i=0}^{2m} \mathcal{W}_i \chi_i, \quad (7)$$

$$\mathbf{P}_{\mathbf{X}\mathbf{X}}^* = \sum_{i=0}^{2m} \mathcal{W}_i [\chi_i - \bar{\mathbf{X}}] [\chi_i - \bar{\mathbf{X}}]^T, \quad (8)$$

where  $\mathcal{W}_i = \lambda/(m + \lambda)$  if  $i = 0$ , otherwise  $\mathcal{W}_i = 1/(2(m + \lambda))$ .

With (7) and (8), the sigma points in (6) are updated. Mapping  $\chi_i$  into (5), the unscented transform for the  $i$ th sigma point is  $\varphi_i = h(\chi_i, \xi) + \mathbf{r}$ . Accordingly, the priori measurement estimation is approximated as  $\bar{\varphi} = \sum_{i=0}^{2m} \mathcal{W}_i \varphi_i + \mathbf{r}$ . Then, the predicted measurement covariance matrix  $\mathbf{P}_{\varphi\varphi}$  and the cross-covariance matrix  $\mathbf{P}_{\mathbf{X}\varphi}$  are updated as

$$\begin{aligned} \mathbf{P}_{\varphi\varphi} &= \sum_{i=0}^{2m} \mathcal{W}_i [\varphi_i - \bar{\varphi}] [\varphi_i - \bar{\varphi}]^T + \mathbf{R}, \\ \mathbf{P}_{\mathbf{X}\varphi} &= \sum_{i=0}^{2m} \mathcal{W}_i [\chi_i - \bar{\mathbf{X}}] [\varphi_i - \bar{\varphi}]^T. \end{aligned} \quad (9)$$

The Sage-Husa estimator [15] is applied to estimate the statistical parameters, i.e.,

$$\begin{aligned} \mathbf{r} &= (1 - \mu)\mathbf{r}_o + \mu \left( \varphi - \sum_{i=0}^{2m} \mathcal{W}_i h(\chi_i, \xi) \right), \\ \mathbf{R} &= (1 - \mu)\mathbf{R}_o + \mu \left[ (\varphi - \bar{\varphi})(\varphi - \bar{\varphi})^T \right. \\ &\quad \left. - \sum_{i=0}^{2m} \mathcal{W}_i (\varphi_i - \bar{\varphi})(\varphi_i - \bar{\varphi})^T \right], \end{aligned} \quad (10)$$

where  $\mu \in [0, 1]$  is the estimation weight.  $\mathbf{r}_o$  and  $\mathbf{R}_o$  denote the priori values of the mean value and variance, respectively.

*Step 3. Rough calculation:* Accordingly, the rough Jacobian matrix  $\tilde{\mathbf{H}}$  can be calculated by  $\tilde{\mathbf{H}} = (\mathbf{P}_{\mathbf{X}\varphi})^T (\mathbf{P}_{\mathbf{X}\mathbf{X}}^*)^{-1}$ . With the linear measurement  $\varphi \triangleq \tilde{\mathbf{H}}\mathbf{X} + \mathbf{W}$ , an iterative least squares method is given to estimate the position, i.e.,

$$(\hat{x}_o, \hat{y}_o)^T = (\hat{x}_{oo}, \hat{y}_{oo})^T + (\tilde{\mathbf{H}}^T \tilde{\mathbf{H}})^{-1} \tilde{\mathbf{H}}^T [\varphi - h(\hat{\mathbf{X}}, \xi)], \quad (11)$$

where  $\tilde{\mathbf{H}}$  is the first two columns of  $\tilde{\mathbf{H}}$ , and  $\hat{\mathbf{X}} = (\hat{x}_o, \hat{y}_o, z_o)$  is the estimation of  $\mathbf{X}$ .  $\hat{x}_{oo}$  and  $\hat{y}_{oo}$  are the priori values of  $\hat{x}_o$  and  $\hat{y}_o$ , respectively. If  $\|(\tilde{\mathbf{H}}^T \tilde{\mathbf{H}})^{-1} \tilde{\mathbf{H}}^T [\varphi - h(\hat{\mathbf{X}}, \xi)]\| < \varepsilon$  is held, the iteration is stopped, where  $\varepsilon$  is a positive decimal.

*Step 4. Precision compensation:* Note that the accuracy of  $\tilde{\mathbf{H}}$  is related with the prior information of  $\mathbf{X}$ . In order to reduce the model errors, the rough position  $(\hat{x}_o, \hat{y}_o)$  in (11) can be considered as the prior mean of  $\mathbf{X}$ , and the covariance matrix is computed by  $\mathbf{P}_{\mathbf{X}\mathbf{X}} = \mathbf{P}_{\mathbf{X}\mathbf{X}}^* - \mathbf{P}_{\mathbf{X}\varphi} (\mathbf{P}_{\varphi\varphi})^{-1} \mathbf{P}_{\varphi\mathbf{X}}^T$ . Substituting the corrected prior information into Step 1 and Step 2, an accurate Jacobian matrix  $\mathbf{H}$  can be obtained, i.e.,

$$\mathbf{H} = (\bar{\mathbf{P}}_{\mathbf{X}\varphi})^T \bar{\mathbf{P}}_{\mathbf{X}\mathbf{X}}^{-1} = \gamma \tilde{\mathbf{H}}, \quad (12)$$

where  $\bar{\mathbf{P}}_{\mathbf{X}\varphi}$  and  $\bar{\mathbf{P}}_{\mathbf{X}\mathbf{X}}$  are the compensated cross-covariance and covariance matrices, respectively. Particularly,  $\gamma = \tilde{\mathbf{H}} \tilde{\mathbf{H}}^\dagger$  represents the compensation instrumental matrix, where  $\dagger$  stands for the pseudo-inverse of a matrix.

Similar to Step 3, an accurate position of ordinary node can be acquired by using the iterative least squares method.

## B. Performance Analysis

*1) Convergence of the Iterative Squares Estimator:* It is denoted that  $\tilde{\mathbf{X}}^* = (\hat{x}_o, \hat{y}_o)^T$ , and its  $k$ th iteration is  $\tilde{\mathbf{X}}_k^*$ . Meanwhile, it is assumed that  $\tilde{\mathbf{H}}$  is full-rank and Lipschitz continuous in a neighborhood of the optimal solution  $\tilde{\mathbf{X}}^*$ .

*Theorem 1:* Consider (11) with  $\tilde{\mathbf{X}}_k^*$ , if  $\tilde{\mathbf{X}}_k^*$  sufficiently closes to  $\tilde{\mathbf{X}}^*$ , the rate of the convergence is quadratic.

*Proof:* Denote  $\varsigma = (\tilde{\mathbf{H}}_k^T \tilde{\mathbf{H}}_k)^{-1} \tilde{\mathbf{H}}_k^T [\varphi - h(\tilde{\mathbf{X}}_k, \xi)]$  and  $f(\tilde{\mathbf{X}}_k^*) = \frac{1}{2} [\varphi - h(\tilde{\mathbf{X}}_k, \xi)]^T [\varphi - h(\tilde{\mathbf{X}}_k, \xi)]$ , where  $\tilde{\mathbf{H}}_k$  and  $\tilde{\mathbf{X}}_k$  are the  $k$ th iteration of  $\tilde{\mathbf{H}}$  and  $\tilde{\mathbf{X}}$ . Then, we have

$$\begin{aligned} \tilde{\mathbf{X}}_k^* + \varsigma - \tilde{\mathbf{X}}^* &= \tilde{\mathbf{X}}_k^* - \tilde{\mathbf{X}}^* + (\tilde{\mathbf{H}}_k^T \tilde{\mathbf{H}}_k)^{-1} \tilde{\mathbf{H}}_k^T [\varphi - h(\tilde{\mathbf{X}}_k, \xi)] \\ &= (\tilde{\mathbf{H}}_k^T \tilde{\mathbf{H}}_k)^{-1} \{ \tilde{\mathbf{H}}_k^T \tilde{\mathbf{H}}_k (\tilde{\mathbf{X}}_k^* - \tilde{\mathbf{X}}^*) + \nabla f(\tilde{\mathbf{X}}^*) - \nabla f(\tilde{\mathbf{X}}_k^*) \}. \end{aligned} \quad (13)$$

Based on the Talor's Theorem in [16], we obtain  $\nabla f(\tilde{\mathbf{X}}^*) - \nabla f(\tilde{\mathbf{X}}_k^*) = \int_0^1 [\tilde{\mathbf{H}}_k^T (\tilde{\mathbf{X}}_k^* + \kappa(\tilde{\mathbf{X}}^* - \tilde{\mathbf{X}}_k^*)) \tilde{\mathbf{H}}_k (\tilde{\mathbf{X}}_k^* + \kappa(\tilde{\mathbf{X}}^* - \tilde{\mathbf{X}}_k^*))] (\tilde{\mathbf{X}}^* - \tilde{\mathbf{X}}_k^*) d\kappa$ , where  $\kappa \in (0, 1)$ .

It is noticed that,  $\tilde{\mathbf{H}}$  is Lipschitz continuous in a neighborhood of the optimal solution  $\tilde{\mathbf{X}}^*$ . Hence, we have  $\tilde{\mathbf{H}}_k^T \tilde{\mathbf{H}}_k - \tilde{\mathbf{H}}_k^T (\tilde{\mathbf{X}}_k^* + \kappa(\tilde{\mathbf{X}}^* - \tilde{\mathbf{X}}_k^*)) \tilde{\mathbf{H}}_k (\tilde{\mathbf{X}}_k^* + \kappa(\tilde{\mathbf{X}}^* - \tilde{\mathbf{X}}_k^*)) \leq L\kappa(\tilde{\mathbf{X}}_k^* - \tilde{\mathbf{X}}^*)$ , where  $L$  is a positive constant. With this, one obtains

$$\begin{aligned} &\left\| \tilde{\mathbf{H}}_k^T \tilde{\mathbf{H}}_k (\tilde{\mathbf{X}}_k^* - \tilde{\mathbf{X}}^*) + \nabla f(\tilde{\mathbf{X}}^*) - \nabla f(\tilde{\mathbf{X}}_k^*) \right\| \\ &= \left\| \tilde{\mathbf{H}}_k^T \tilde{\mathbf{H}}_k (\tilde{\mathbf{X}}_k^* - \tilde{\mathbf{X}}^*) + \int_0^1 [\tilde{\mathbf{H}}_k^T (\tilde{\mathbf{X}}_k^* + \kappa(\tilde{\mathbf{X}}^* - \tilde{\mathbf{X}}_k^*)) \right. \\ &\quad \left. \times \tilde{\mathbf{H}}_k (\tilde{\mathbf{X}}_k^* + \kappa(\tilde{\mathbf{X}}^* - \tilde{\mathbf{X}}_k^*))] (\tilde{\mathbf{X}}^* - \tilde{\mathbf{X}}_k^*) d\kappa \right\| \\ &= \left\| \int_0^1 [\tilde{\mathbf{H}}_k^T \tilde{\mathbf{H}}_k - \tilde{\mathbf{H}}_k^T (\tilde{\mathbf{X}}_k^* + \kappa(\tilde{\mathbf{X}}^* - \tilde{\mathbf{X}}_k^*)) \right. \\ &\quad \left. \times \tilde{\mathbf{H}}_k (\tilde{\mathbf{X}}_k^* + \kappa(\tilde{\mathbf{X}}^* - \tilde{\mathbf{X}}_k^*))] (\tilde{\mathbf{X}}_k^* - \tilde{\mathbf{X}}^*) d\kappa \right\| \\ &\leq \left\| \int_0^1 L\kappa (\tilde{\mathbf{X}}_k^* - \tilde{\mathbf{X}}^*)^2 d\kappa \right\| \leq \frac{L}{2} \left\| (\tilde{\mathbf{X}}_k^* - \tilde{\mathbf{X}}^*) \right\|^2. \end{aligned} \quad (14)$$

Submitting (14) into (13), we have  $\|\tilde{\mathbf{X}}_k^* + \varsigma - \tilde{\mathbf{X}}^*\| \leq \frac{1}{2} \tilde{L} \|(\tilde{\mathbf{X}}_k^* - \tilde{\mathbf{X}}^*)\|^2$ , where  $\tilde{L} = L \|(\tilde{\mathbf{H}}_k^T \tilde{\mathbf{H}}_k)^{-1}\|$ , i.e., the rate of convergence for (11) is quadratic with the estimator  $\tilde{\mathbf{X}}_k^*$ . ■

*2) Cramér-Rao Lower Bound:* We drive the Cramér-Rao Lower Bound (CRLB) for the proposed algorithm, which is a lower bound to the error variance. The ground truth is denoted by  $\mathbf{X}^*$ , and the log-likelihood function of the ordinary node is  $\ln \Lambda(\mathbf{X}^*)$ , i.e.,

$$\begin{aligned} \ln \Lambda(\mathbf{X}^*) &= \frac{1}{2} [\varphi - h(\mathbf{X}, \xi) - \mathbf{r}]^T \mathbf{R}^{-1} [\varphi - h(\mathbf{X}, \xi) - \mathbf{r}] \\ &= \frac{1}{2} [\varphi - \mathbf{H}\mathbf{X} - \mathbf{r}]^T \mathbf{R}^{-1} [\varphi - \mathbf{H}\mathbf{X} - \mathbf{r}]. \end{aligned} \quad (15)$$

Then, the Fisher Information Matrix (FIM) is given by

$$\begin{aligned} \mathcal{L}(\mathbf{X}^*) &= E \{ [\nabla_{\mathbf{X}^*} \ln \Lambda(\mathbf{X}^*)] [\nabla_{\mathbf{X}^*} \ln \Lambda(\mathbf{X}^*)]^T \} |_{\mathbf{X}^* = \mathbf{X}^*} \\ &= -E \{ \nabla_{\mathbf{X}^*} \nabla_{\mathbf{X}^*}^T \ln \Lambda(\mathbf{X}^*) \} |_{\mathbf{X}^* = \mathbf{X}^*}. \end{aligned} \quad (16)$$

Based on (15) and (16), the CRLB for  $\mathbf{X}^*$  is given as  $\text{CRLB}(\mathbf{X}^*) = \mathcal{L}^{-1}(\mathbf{X}^*)$ . Particularly, the first two columns of  $\mathbf{H}$  can be denoted by  $\hat{\mathbf{H}}$ , where  $\hat{\mathbf{H}} = [\mathcal{H}_{1,1}, \mathcal{H}_{1,2}; \mathcal{H}_{2,1}, \mathcal{H}_{2,2}; \mathcal{H}_{3,1}, \mathcal{H}_{3,2}; \mathcal{H}_{4,1}, \mathcal{H}_{4,2}; \mathcal{H}_{5,1}, \mathcal{H}_{5,2}; \mathcal{H}_{6,1}, \mathcal{H}_{6,2}]$ . Besides,  $\mathcal{H}_{m,n}$  represents the  $m$ th row and  $n$ th column of  $\hat{\mathbf{H}}$ . With

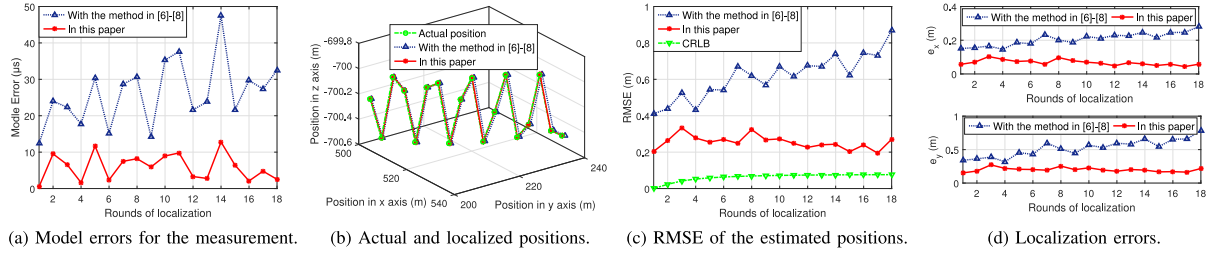


Fig. 2. Simulation results for the localization algorithm with asynchronous clock and stratification effect.

straightforward calculation, we have the following results

$$\begin{aligned} [\mathcal{L}(\mathbf{X}^*)]_{1,1} &= \mathbf{R}^{-1}[(\mathcal{H}_{1,1})^2, (\mathcal{H}_{2,1})^2, (\mathcal{H}_{3,1})^2, \\ &\quad (\mathcal{H}_{4,1})^2, (\mathcal{H}_{5,1})^2, (\mathcal{H}_{6,1})^2]^T \\ [\mathcal{L}(\mathbf{X}^*)]_{2,2} &= \mathbf{R}^{-1}[(\mathcal{H}_{1,2})^2, (\mathcal{H}_{2,2})^2, (\mathcal{H}_{3,2})^2, \\ &\quad (\mathcal{H}_{4,2})^2, (\mathcal{H}_{5,2})^2, (\mathcal{H}_{6,2})^2]^T \\ [\mathcal{L}(\mathbf{X}^*)]_{1,2} &= \mathbf{R}^{-1}[\mathcal{H}_{1,1}\mathcal{H}_{1,2}, \mathcal{H}_{2,1}\mathcal{H}_{2,2}, \mathcal{H}_{3,1}\mathcal{H}_{3,2}, \\ &\quad \mathcal{H}_{4,1}\mathcal{H}_{4,2}, \mathcal{H}_{5,1}\mathcal{H}_{5,2}, \mathcal{H}_{6,1}\mathcal{H}_{6,2}]^T \\ [\mathcal{L}(\mathbf{X}^*)]_{2,1} &= [\mathcal{L}(\mathbf{X}^*)]_{1,2}. \end{aligned}$$

Therefore, the localization error of  $\mathbf{X}^*$  is given by

$$E \left\{ \left\| \hat{\mathbf{X}}^* - \bar{\mathbf{X}}^* \right\|^2 \right\} \geq \text{tr} \{ \mathcal{L}^{-1}(\mathbf{X}^*) \} |_{\mathbf{X}^* = \bar{\mathbf{X}}^*}. \quad (17)$$

#### IV. SIMULATION RESULTS

Simulations are implemented in MATLAB 2017b to validate the effectiveness of the proposed algorithm. Specially, eighteen static points are required to be localized, i.e., ordinary node is sequentially located at eighteen different positions. Some parameters used for the simulation are given as:  $\bar{a} = 0.017$ ,  $b = 1473$  m/s,  $\sigma_{mea} = 0.001$ ,  $\lambda = -2.9997$  and  $\varepsilon = 0.1$ . For the first point,  $\gamma = [0.4046, 0.1963, -0.2083, -0.3303, -0.1603, 0.1700; 0.2051, 0.3876, 0.1825, -0.1675, -0.3165, -0.1490; -0.1995, 0.1913, 0.3908, 0.1629, -0.1562, -0.3191; -0.3303, -0.1603, 0.1700, 0.2697, 0.1309, -0.1388; -0.1675, -0.3165, -0.1490, 0.1367, 0.2584, 0.1217; 0.1629, -0.1562, -0.3191, -0.1330, 0.1275, 0.2605]$ . Initially,  $\mathbf{r} = [\sigma_{mea}^2; \sigma_{mea}^2; \sigma_{mea}^2; \sigma_{mea}^2; \sigma_{mea}^2; \sigma_{mea}^2]$  and  $\mathbf{R} = 0.5 * \text{diag}(\sigma_{mea}^2, \sigma_{mea}^2, \sigma_{mea}^2, \sigma_{mea}^2, \sigma_{mea}^2, \sigma_{mea}^2)$ .

In [6]–[8], the first-order linearization technique is employed to calculate  $\mathbf{H}$ . As mentioned above, the first-order linearization technique can introduce large model error. In order to verify this conclusion, we define the model error as  $e_{\text{model}} = \|h(\mathbf{X}, \xi) - h(\hat{\mathbf{X}}, \xi) - \mathbf{H}(\mathbf{X} - \hat{\mathbf{X}})\|$ . Then, the model errors with different strategies are shown in Fig. 2(a). It is clear that, the model error in this letter is smaller than the ones in [6]–[8]. This comparison reflects that the unscented transform strategy in this letter is meaningful and necessary.

With Jacobian matrix, the position of the ordinary node is calculated through the iterative least squares method. For comparison, the first-order linearization technique is also applied to the iterative least squares method. Of note, this design is similar to the scenario in [6]–[8]. Accordingly, the actual and estimated positions of the eighteen different points are shown in Fig. 2(b). The localization performance is evaluated by root mean square errors (RMSE), and the RMSE is defined by

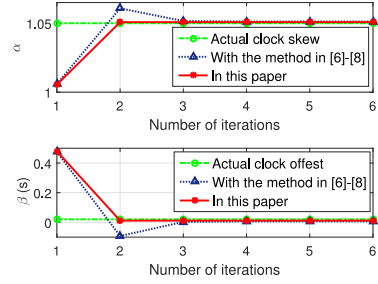


Fig. 3. Estimated time clock for one round of localization.

$e_{\text{RMSE}} = [\frac{1}{N} \sum_{i=1}^N \|X - \hat{X}\|_i^2]^{0.5}$ , where  $N$  is the number of Monte Carlo runs. Through this definition, the RMSE is shown in Fig. 2(c). To show more clearly, we present the localization error on each axis. As the ordinary node is equipped with depth units, then the localization error on the depth can be omitted. In respect that, the localization errors on the x axis and the y axis are defined by  $e_x = \frac{1}{N} \sum_{i=1}^N |x_o - \hat{x}_o|_i$  and  $e_y = \frac{1}{N} \sum_{i=1}^N |y_o - \hat{y}_o|_i$ , respectively. Correspondingly, the localization errors are shown in Fig. 2(d). From Fig. 2(c) and Fig. 2(d), we know the algorithm in this letter can improve the localization accuracy. Meanwhile, the RMSE in this letter is closer to the theoretical CRLB as compared with the first-order linearization technique based algorithms, e.g., [6]–[8].

It is interesting to find that, the time clock (i.e.,  $\alpha$  and  $\beta$ ) has no effect on the performance of localization algorithm. However, the clock can serve as an auxiliary way to verify the effectiveness of the localization algorithm. Inspired by this, the input-output relationship for  $\alpha$  and  $\beta$  is denoted as  $\bar{\mathbf{B}} = \bar{\mathbf{A}}\bar{\mathbf{C}} + \bar{\mathbf{W}}$ , where  $\bar{\mathbf{B}} = [T_{o,o}, T_{o,o}, T_{o,o}, T_{1,o}, T_{2,o}, T_{3,o}]^T$ ,  $\bar{\mathbf{A}} = [t_{o,1} - \tau_{o,1}, 1; t_{o,2} - \tau_{o,2}, 1; t_{o,3} - \tau_{o,3}, 1; t_{1,1} - \tau_{1,o}, 1; t_{2,2} - \tau_{2,o}, 1; t_{3,3} - \tau_{3,o}, 1]$ ,  $\bar{\mathbf{C}} = [\alpha, \beta]^T$ , and  $\bar{\mathbf{W}} \in \mathcal{R}^{6 \times 1}$  is the measurement noise. By employing the least squares method, the time clock can be estimated as  $\bar{\mathbf{C}} = (\bar{\mathbf{A}}^T \bar{\mathbf{A}})^{-1} \bar{\mathbf{A}}^T \bar{\mathbf{B}}$ . Based on this, the estimated clock information at an arbitrary round of localization is represented in Fig. 3. Clearly, the clock information can be well estimated, which indirectly verifies the effectiveness of localization algorithm.

#### V. CONCLUSION

This letter studies the asynchronous joint localization issue for UASNs. An unscented transform based algorithm has been presented. Instead of linearization technique required by the existing works, the unscented transform does not need to compute the derivation of the Jacobian matrix. Simulation results shows that the proposed algorithm can reduce the linearization errors, and hence the estimation accuracy is improved.



## REFERENCES

- [1] S. Jiang, "On reliable data transfer in underwater acoustic networks: A survey from networking perspective," *IEEE Commun. Surv. Tut.*, vol. 20, no. 1, pp. 1036–1055, May 2018.
- [2] Y. Zou, H. Liu, and Q. Wan, "Joint synchronization and localization in wireless sensor networks using semidefinite programming," *IEEE Internet Things J.*, vol. 5, no. 1, pp. 199–205, Feb. 2018.
- [3] Y. Liu, Y. Shen, D. Guo, and M. Win, "Network localization and synchronization using full-duplex radios," *IEEE Trans. Signal Process.*, vol. 66, no. 3, pp. 714–728, Feb. 2018.
- [4] F. Meyer, B. Etxlinger, Z. Liu, F. Hlawatsch, and M. Win, "A scalable algorithm for network localization and synchronization," *IEEE Internet Things J.*, vol. 5, no. 6, pp. 4714–4727, Dec. 2018, doi: [10.1109/JIOT.2018.2811408](https://doi.org/10.1109/JIOT.2018.2811408).
- [5] F. Zhang, G. Wang, and W. Wang, "Novel two-step method for joint synchronization and localization in asynchronous networks," *IEEE Wireless Commun. Lett.*, vol. 6, no. 6, pp. 830–833, Dec. 2017.
- [6] J. Liu, Z. Wang, J. Cui, S. Zhou, and B. Yang, "A joint time synchronization and localization design for mobile underwater sensor networks," *IEEE Trans. Mobile Comput.*, vol. 15, no. 3, pp. 530–543, Mar. 2016.
- [7] E. Mortazavi, R. Javidan, M. Dehghani, and V. Kavooosi, "A robust method for underwater wireless sensor joint localization and synchronization," *Ocean Eng.*, vol. 137, no. 1, pp. 276–286, Jun. 2017.
- [8] B. Zhang, H. Wang, L. Zheng, J. Wu, and Z. Zhuang, "Joint synchronization and localization for underwater sensor networks considering stratification effect," *IEEE Access*, vol. 5, pp. 26932–26943, 2017.
- [9] Z. Gong, C. Li, and F. Jiang, "AUV-aided joint localization and time synchronization for underwater acoustic sensor networks," *IEEE Signal Process. Lett.*, vol. 25, no. 4, pp. 477–481, Apr. 2018.
- [10] J. Yan, X. Zhang, X. Luo, Y. Wang, C. Chen, and X. Guan, "Asynchronous localization with mobility prediction for underwater acoustic sensor networks," *IEEE Trans. Veh. Technol.*, vol. 67, no. 3, pp. 2543–2556, Mar. 2018.
- [11] P. Carroll, K. Mahmood, S. Zhou, H. Zhou, X. Xu, and J. Cui, "On demand asynchronous localization for underwater sensor networks," *IEEE Trans. Signal Process.*, vol. 62, no. 13, pp. 3337–3348, Jul. 2014.
- [12] S. Julier, J. Uhlmann, and H. Durrantwhyte, "A new method for non-linear transformation of means and covariances in filters and estimates," *IEEE Trans. Autom. Control*, vol. 45, no. 3, pp. 477–482, Mar. 2000.
- [13] J. Yan, Z. Xu, X. Luo, C. Chen, and X. Guan, "Feedback-based target localization in underwater sensor networks: A multi-sensor fusion approach," *IEEE Trans. Signal Inf. Process. Netw.*, vol. 5, no. 1, pp. 168–180, Mar. 2019.
- [14] H. Ramezani, H. Jamali-Rad, and G. Leus, "Target localization and tracking for an isogradient sound speed profile," *IEEE Trans. Signal Process.*, vol. 61, no. 6, pp. 1434–1446, Mar. 2013.
- [15] Y. Shi, C. Han, and Y. Liang, "Adaptive UKF for target tracking with unknown process noise statistics," in *Proc. Int. Conf. Inf. Fusion*, Seattle, WA, USA, Jul. 2009, pp. 1815–1820.
- [16] J. Nocedal and S. Wright, *Numerical Optimization*. New York, NY, USA: Springer, 2006.